

Dynamic screening in a two-species asymmetric exclusion process

Kyung Hyuk Kim and Marcel den Nijs

Department of Physics, University of Washington, Seattle, Washington 98195, USA

(Received 9 May 2007; published 6 August 2007)

The dynamic scaling properties of the one-dimensional Burgers equation are expected to change with the inclusion of additional conserved degrees of freedom. We study this by means of one-dimensional (1D) driven lattice gas models that conserve both mass and momentum. The most elementary version of this is the Arndt-Heinzel-Rittenberg (AHR) process, which is usually presented as a two-species diffusion process, with particles of opposite charge hopping in opposite directions and with a variable passing probability. From the hydrodynamics perspective this can be viewed as two coupled Burgers equations, with the number of positive and negative momentum quanta individually conserved. We determine the dynamic scaling dimension of the AHR process from the time evolution of the two-point correlation functions, and find numerically that the dynamic critical exponent is consistent with simple Kardar-Parisi-Zhang- (KPZ) type scaling. We establish that this is the result of perfect screening of fluctuations in the stationary state. The two-point correlations decay exponentially in our simulations and in such a manner that in terms of quasiparticles, fluctuations fully screen each other at coarse grained length scales. We prove this screening rigorously using the analytic matrix product structure of the stationary state. The proof suggests the existence of a topological invariant. The process remains in the KPZ universality class but only in the sense of a factorization, as $(\text{KPZ})^2$. The two Burgers equations decouple at large length scales due to the perfect screening.

DOI: [10.1103/PhysRevE.76.021107](https://doi.org/10.1103/PhysRevE.76.021107)

PACS number(s): 64.60.Ht, 05.40.-a, 05.70.Ln, 44.10.+i

I. INTRODUCTION

Many nonequilibrium driven systems display scale invariance in their stationary states, i.e., strongly correlated collective structures without a characteristic length scale limiting the fluctuations. Such correlations typically decay as power laws with critical exponents that are universal. Their values depend only on global issues such as dimensionality, symmetry, and specific microscopic conservation laws. The classification of dynamic universality classes and the determination of their scaling dimensions is one of the central issues in current research of nonequilibrium statistical physics [1,2]. The one-species asymmetric exclusion processes (ASEP) serves in this context as both the simplest prototype model for driven one-dimensional (1D) stochastic particle flow [3–5] and as a fully discretized version of the 1D Burgers equation (with time and space discretized, and momentum quantized) [6].

In this paper we investigate how the properties of such stochastic flows change with the introduction of additional bulk conservation laws. The generic expectation is that enforcing more conservation laws changes the scaling dimensions. We follow a bottom-up approach. An example of a top-down approach is the current interest in anomalous 1D heat conduction in Fermi-Pasta-Ulam-type models (e.g., a chain of anharmonic oscillators [7], or a one-dimensional gas of particles in a narrow channel with different types of interactions [8]). The systems are coupled to heat reservoirs on either end. Those are held at different temperatures and thus induce heat flow along the channel. Computer simulations, e.g., using molecular dynamics, show an anomalous thermal conductivity κ , $J_Q \approx \kappa \nabla T$, diverging with system size L as $\kappa \sim L^\alpha$. The numerical estimates for the value of α in the various versions of the process vary between $0.22 < \alpha < 0.44$ [7–9]. α is expected to be universal. From the ana-

lytic side, a mode-coupling treatment predicted $\alpha=2/5$ [10], while a renormalization analysis of the full hydrodynamic equations predicts $\alpha=1/3$, based on Galilean invariance and an assumption of local equilibrium in the heat sector [11]. In our study we add conservation laws to the Burgers equation instead of coarse graining down from full hydrodynamics.

The equivalences between ASEP, KPZ growth, and the Burgers equation are well known [6]. ASEP is usually interpreted as a process for stochastic particle transport, while the Burgers equation

$$\frac{\partial v}{\partial t} = \frac{\partial}{\partial x} \left[v \frac{\partial v}{\partial x} + \lambda v^2 + \eta(x, t) \right] \quad (1)$$

represents the evolution of a (vortex-free) velocity field $v(x, t)$, and conserves momentum only [12]. The interpretation of ASEP as a fully discretized Burgers equation poses some conceptual issues. Due to the full quantization of the momenta in ASEP, in units of $n=0, 1$, it can appear that the process also conserves energy. A careful discussion [13] shows that energy is conserved between updates but fluctuates during each update. Therefore ASEP is a genuine fully discretized implementation of the Burgers equation from this direct point of view as well. In Sec. II we discuss how to impose conservation of particles in addition to conservation of momentum. This leads naturally to the two-species ASEP known as the Arndt-Heinzel-Rittenberg (AHR) model [14,15]. This process has been the focus of intensive studies, but its dynamic scaling properties seem to have been ignored. Instead, the stationary state properties have been center stage, in particular, its clustering, and that it can be constructed exactly using the so-called matrix product ansatz method [16–20].

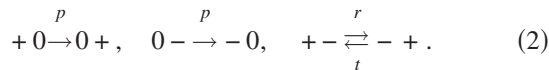
We establish that the introduction of this additional conservation law to ASEP does not change the universality class,

but it does so in a rather intricate manner. KPZ scaling changes to $(\text{KPZ})^2$ -type scaling. The AHR process can be interpreted as a coupled Burgers and diffusion equation, conserving both mass and momentum; or as two coupled Burgers equations, one for positive and negative momentum quanta, separately. The latter point of view turns out to be the most productive. At large length scales the coupling vanishes and the process factorizes, in terms of quasiparticles, into two decoupled Burger processes. This is achieved by means of perfect screening of fluctuations in the stationary state. We observe this numerically from the behavior of the two-point correlators (Secs. IV and V). The stationary state of the model is known to satisfy the so-called matrix product ansatz [14]. We use that property to prove analytically that the perfect screening is rigorous (Sec. VI). In Secs. IV and V we present also direct numerical evidence that the dynamic critical exponent is indeed the same as in KPZ, $z=3/2$, using the time evolution of the two point correlators. The conventional methods fail due to time oscillations. This might be the first example of such a numerical dynamic analysis in terms of correlation functions.

II. AHR MODEL

Our aim is to construct a generalization of ASEP describing a process where particle diffusion and the Burgers equation are coupled to each other. Energy will not be conserved. The particles in such a model need to carry an internal degree of freedom, representing momentum. A site could be in four states. It would be empty ($n_x=0$) or be occupied by a particle ($n_x=1$) with momentum $v_x=+1, 0, -1$. Particles with $+1$ (-1) momentum would hop with a right (left) bias. Some reflection on the nature of the passing processes (the collisions) shows that we can remove the zero-momentum state of particles, without loss of generality [13].

This then leads naturally to the two-species ASEP known as the Arndt-Heinzel-Rittenberg (AHR) model. The conventional interpretation of this process is in terms of diffusion of charged particles in an electric field. Two species of particles with opposite unit charge hop in opposite directions along a 1D lattice ring, driven by the electric field.



Each site x can be in three states, $S_x=0, \pm 1$, with $S=1$ ($S=-1$) representing the right (left) moving species and $S=0$ an empty site. p is the free directed hopping rate (the electric field) and r the passing rate of opposite charged particles. In our study, the numbers of $S=1$ and $S=-1$ particles on the ring are chosen to be equal. Compared to the conventional single species ASEP, this process has two local conservation laws instead of one; both species are conserved independently.

In the coupled diffusion-Burgers equation interpretation of the same process, the charge represents a quantum of momentum moving in the opposite direction as illustrated in Fig. 1. No driving force is present, because the preferred hopping direction represents the total derivative in the

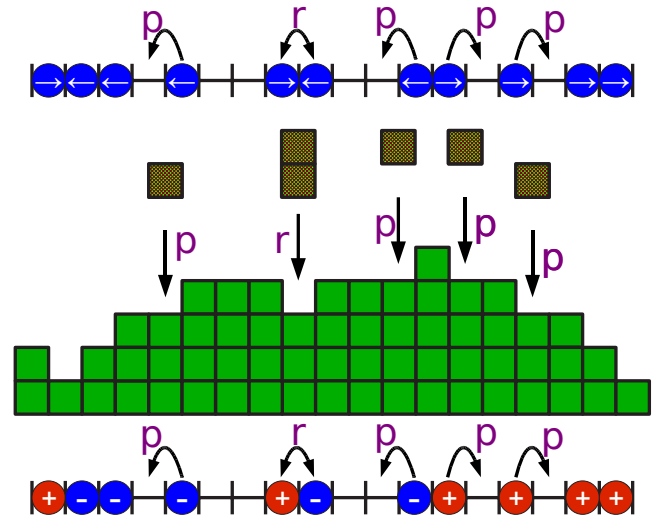


FIG. 1. (Color online) Two-species asymmetric exclusion process (bottom) and its corresponding interface growth model (middle) and particle flow model with momentum conservation (top).

Navier-Stokes equation, just as in the single species ASEP. Similar to ASEP, energy is not a conserved quantity: The energy of particles is conserved between updates but fluctuates during the updates. That leaves particles in different places than where they would have been if energy were conserved [13].

The AHR model reduces to the $S_x=\pm 1$ spin (momentum quanta) representation of ASEP in the high density limit where vacant sites $S=0$ are absent. There, the particle density cannot fluctuate anymore, and the process falls thus back to the Burgers equation with only one conservation law. This limit is singular. The AHR process is not the generic $S=0, \pm 1$ generalization of ASEP in the sense of the KPZ and Burgers equation. The proper generalization would be the so-called restricted solid-on-solid (RSOS) model (Kim-Kosterlitz model) where $+$ and $-$ pairs can be annihilated and created. Those processes conserve momentum. The $S=+1$ ($S=-1$) particles represent up (down) steps in the KPZ-type interface; the free hopping rate p represents step flow. Growth at flat terraces is blocked in the AHR process, except for the deposition of vertical dimers (with rate r) in single-particle puddles. Figure 1 illustrates this.

This means that from the KPZ point of view the AHR process represents a growing interface where the number of up and down steps are individually preserved. Whether this local conservation law changes the scaling dimensions on large scales is the central issue we address here. From the KPZ perspective, your initial guess would probably be “no,” and from the lattice gas perspective, “yes.” Our results presented below confirm the “no,” but in a rather subtle manner, the universality class is “ $(\text{KPZ})^2$ ” instead of simple KPZ.

The AHR model has been widely studied recently, with as focus the structure of its stationary state [14–19]. We are not aware of any previous dynamic scaling analysis. The stationary state shows strong clustering, as a function of decreasing passing versus free hopping probability r/p . Stretches of “empty” road are followed by high density clusters. These

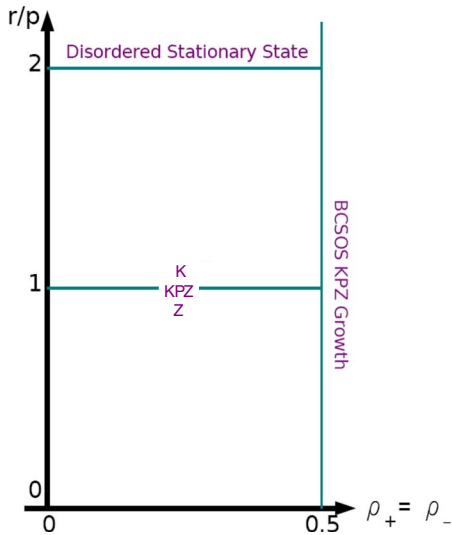


FIG. 2. (Color online) Phase diagram for the AHR model as a function of r/p and (conserved) average density $\rho = \rho_+ = \rho_-$.

are mixtures of $S = +1$ and $S = -1$ particles. We will identify the amount of mixing with the quasiparticles and the cluster size with the screening length.

The passing of $+$ and $-$ particles resembles collisions. The ratio r/p controls the duration of the collision (the softness of the balls). This passing delay creates queuing and is the origin of the clustering. The full AHR model includes a reverse-passing probability t , $[(-+) \rightarrow (+-)]$; particles switching position in the direction opposite to the electric field]. That enhances the clustering even more. We limit ourselves here to the $t=0$ version of the model.

The clustering extends over such large length scales, in specific ranges of r/p and t/p , that the possibility of a phase transition into a macroscopic clustered stationary state has been the major issue [14,15]. Macroscopic cluster condensation (infinite-sized clusters) have been shown to be impossible using the analytic matrix product ansatz [17] and also using an approximate mapping onto the so-called zero-range process [16]. The cluster size remains always finite, but the maximum value can be far beyond all computation capabilities [17].

III. PHASE DIAGRAM

Figure 2 shows the phase diagram of the $t=0$ AHR model as a function of r/p and (conserved) global average density $\rho = \rho_+ = \rho_-$. It contains three special lines: $r/p=1$, $r/p=2$, and $\rho=0.5$, respectively.

Along the $\rho=1/2$ line all sites are fully occupied and the process reduces to the single-species ASEP. From the perspective of the AHR process as modeling two coupled conserved degrees of freedom, momentum and density, the density sector freezes out, leaving only the Burgers equation. The $\rho=1/2$ limit is therefore anomalous, and this line is not the proper backbone of the phase diagram. The dynamic scaling exponent is equal to $z=3/2$ along this line, but that does not need to extend to $\rho < 0.5$.

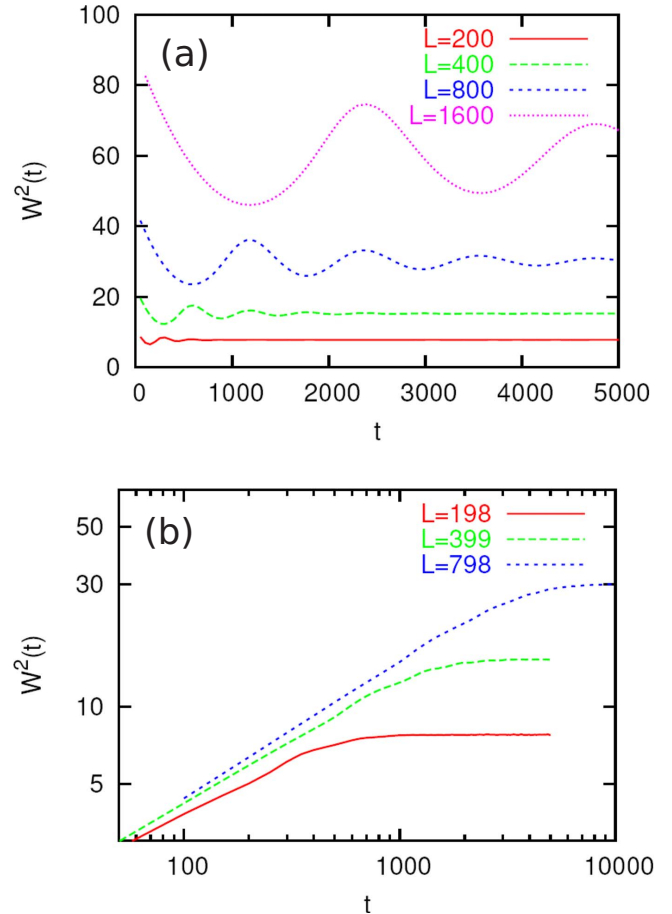


FIG. 3. (Color online) The evolution of interface widths with uncorrelated disordered initial states with $r=p=1.0$ and $\rho=0.25$ (a) and flat initial states with $r=p=1.0$ and $\rho=1/3$ (b) for different system sizes L .

The $r/p=1$ line and the interpretation of the AHR process in terms of two coupled Burgers equations form the true backbone of the phase diagram. At $r=p$, the process reduces to a single-species ASEP in two different ways. If the $+$ particles choose to be blind to the difference between an empty site and a $-$ particle, they see at $r=p$ no difference between a free hop and a passing event, and thus experience pure single species ASEP scaling. The same is true in the projected subspace where $-$ particles are blind to the difference between empty sites and $+$ particles. These subspaces are not perpendicular and the process does not factorize into two independent ASEP processes. Correlations exist between the $+$ and $-$ particles, resulting in clustering. We will study this numerically in the next section and find that at large length scales the process factorizes after all, into $(KPZ)^2$.

At $r \neq p$ the particles can still pretend to be blind to the other species, but then experience updates where the hopping probability inexplicably changes from p to r . These events are random, but not uncorrelated. For $r < p$ the clustering increases and for $r > p$ decreases. The line $r=2p$ is special; there the clustering vanishes accidentally altogether.

IV. DYNAMIC PERFECT SCREENING AT $r=p$

Our investigation of dynamic scaling in the AHR model started with an attempt to measure the dynamic critical ex-

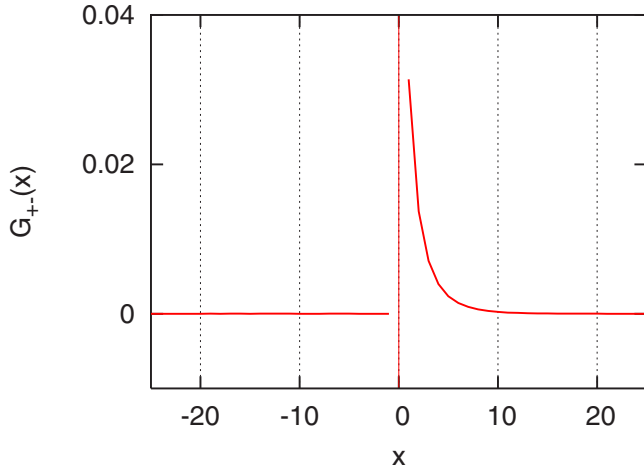


FIG. 4. (Color online) $\mathcal{G}_{+-}(x)$ in the stationary state with $r=p$, $\rho=0.25$, and $L=800$.

ponent z in the conventional manner, i.e., from the time evolution of the interface width starting from a flat or a random initial state. Recall that the AHR model is a RSOS-type KPZ growth model with a conserved number of up and down steps. It turns out that this interface width oscillates in time while evolving toward the stationary state, as illustrated in Fig. 3.

The flat initial state evolves roughly in accordance with conventional scaling, i.e., as $W \sim t^\beta$, with $\beta = \alpha/z$, at intermediate times and saturating at $W \sim L^\alpha$ (with α the stationary state roughness exponent), but the oscillations on top of this behavior are too strong to accurately determine β . These oscillations reflect the additional conservation law, and are tied to traveling wave packets propagating in opposite directions and meeting again after traveling around the lattice ring.

For the resolution of this problem we turn our attention towards these wave packets themselves, by monitoring the manner they spread in time. This is achieved in terms of the two-point correlators

$$\mathcal{G}_{+-}(x,t) = \langle n_+(0)n_-(x) \rangle - \langle n_+(0) \rangle \langle n_-(x) \rangle, \quad (3)$$

and \mathcal{G}_{++} and \mathcal{G}_{--} , where $n_\pm(x)$ is the number operator for \pm particles at site x and at time t . The perfect screening phe-

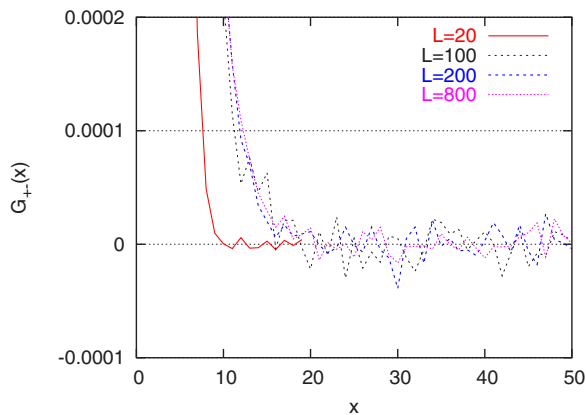


FIG. 5. (Color online) Offsets of $\mathcal{G}_{+-}(x)$ in stationary states for $L=20,100,200,800$ with $\rho=0.25$.

nomenon in the stationary state emerged while we tested this method. In this section we first present and discuss perfect screening and then present the numerical analysis of the dynamic exponent, both at $r=p$.

A. Stationary-state correlation functions

In the stationary state, the correlation function

$$\mathcal{G}_{+-}(x) = \langle n_+(0)n_-(x) \rangle - \rho^2 \quad (4)$$

decays exponentially toward zero. Figures 4 and 5 illustrate this, using Monte Carlo (MC) simulations for periodic boundary conditions for small rings, $L \leq 800$. The correlation function decays exponentially for $x > 0$ and is zero for $x < 0$. Correlations are absent at $x < 0$, because after passing, $-$ and $+$ particles hop away from each other, and (at $r=p$) do not communicate with each other anymore.

The correlation length is rather short in Fig. 4, $\xi \approx 5$, but increases with density along the $r=p$ line. The most significant aspect is not the correlation length, but the absence of any finite-size scaling offset $\mathcal{G}_{+-}(x) \sim B/L$ for $x \gg \xi$ and $x < 0$.

The absence of this offset is quite surprising. It indicates a “perfect screening” localization-type phenomenon in the fluctuations. To appreciate this, consider the two-point correlation in a random disordered state, such as the single species ASEP stationary state. The \mathcal{G}_{++} and \mathcal{G}_{--} correlators in our model have exactly that form at $r=p$ because each couples only to one of the two projected single-species ASEP subspaces. Such correlators are δ functions (with negative $\mathcal{G}(0)/L$ offsets) because periodic boundary conditions imply rigorous global conservation of the total number of particles, and impose the condition that the total area underneath $\mathcal{G}(x)$ is exactly equal to zero.

Another way of viewing this starts by realizing that $\mathcal{G}_{+-}(x)/\rho$ can be interpreted as the probability to find a $-$ particle at distance x from a tagged $+$ particle at site x_0 . The tagging removes an amount of probability ρ from x_0 corresponding to the (untagged) probability of finding a $-$ particle at x_0 . This amount is redistributed over the chain. In general, we would expect that part of this expelled probability remains localized near x_0 , represented in \mathcal{G}_{+-} by the area underneath the exponential; and that the remainder is distributed uniformly over the chain in delocalized form, represented by a uniform B/L -type finite size offset in \mathcal{G}_{+-} . For uncorrelated δ -function-type correlations all of it is delocalized, such that $B = \rho^2$. Our numerical simulations, see Fig. 5, put a bound on the delocalized amplitude; e.g., $|B|/L < 8 \times 10^{-6}$ at $L=800$ for $\rho=0.25$. The delocalized fraction is zero within the MC noise.

So surprisingly, in our process all the excluded probability is localized, such that

$$\mathcal{G}_{+-}(0) = - \sum_{y=1}^{y=a} \mathcal{G}_{+-}(y) \quad (5)$$

for all $\xi \ll a \ll L$. A person riding on top of a specific $+$ particle and wearing glasses that filter out the $-$ particles, observes a perfect single-species ASEP in terms of the $+$ par-

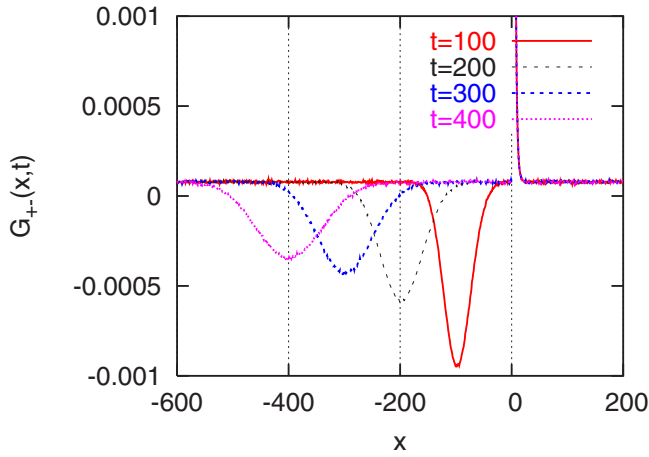


FIG. 6. (Color online) $\mathcal{G}_{+-}(x,t)$ at a series of time $t=100, 200, 300, 400$ with $r=p=1.0$, $\rho=0.25$, and $L=800$. The group velocity is equal to $v_g=2p(1-2\rho)=1$.

ticles. Without glasses she notices, however, an excess of $-$ particles in front of her. This cloud of size ξ has on average an excess mass equal to ρ .

B. Factorization from perfect screening

The above perfect screening implies that the AHR process at $r=p$ behaves at coarse grained scales as two decoupled single-species Burgers equations. This factorization is easily recognized in the interface growth representation. Recall that the $+$ particles represent up steps and the $-$ particles down steps, and that the number of both are conserved. Perfect screening means factorization into two decoupled KPZ interface growth processes at length scales $x \gg \xi$ (one where down steps are being ignored and the other where the up steps are ignored).

The interface width $W(x)$ of the full model over a section of the interface of length x can be expressed in terms of the two-point correlators as

$$\begin{aligned} W(x)^2 &\equiv \langle (h(x) - h(0))^2 \rangle = \left\langle \left(\sum_{y=0}^x (-n_+(y) + n_-(y)) \right)^2 \right\rangle \\ &= \left\langle \left(\sum_{y=0}^x (n_+ - \rho_+) - \sum_{z=0}^x (n_- - \rho_-) \right)^2 \right\rangle \\ &= \sum_{y,z=0}^x [\mathcal{G}_{++}(y-z) + \mathcal{G}_{--}(y-z) \\ &\quad - \mathcal{G}_{+-}(y-z) - \mathcal{G}_{-+}(y-z)]. \end{aligned} \quad (6)$$

\mathcal{G}_{++} and \mathcal{G}_{--} are δ functions at $r=p$ and their finite-size offsets are absent in the thermodynamic limit $L \rightarrow \infty$,

$$W(x)^2 = x(\rho_+ - \rho_+^2) + x(\rho_- - \rho_-^2) + 2x(\rho^2 - A_{+-}).$$

Moreover, at length scales much larger than the screening length, $x \gg \xi$, the cross-correlator area $A_{+-} \equiv \sum_{y=1}^x \mathcal{G}_{+-}(y)$ reduces to $A_{+-} = \rho^2$ by perfect screening, such that the \mathcal{G}_{+-} contributions vanish completely.

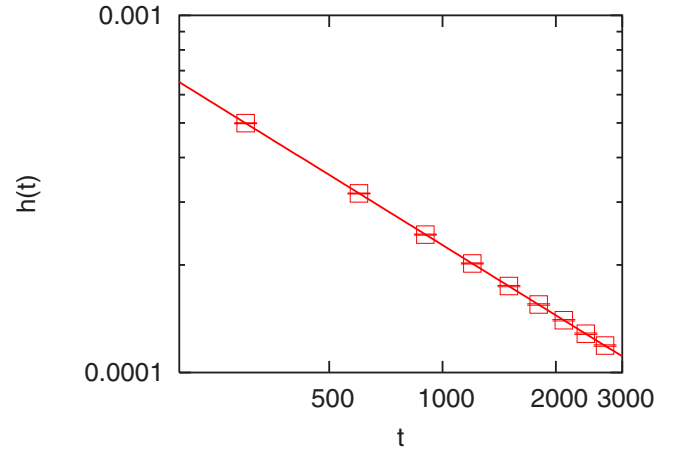
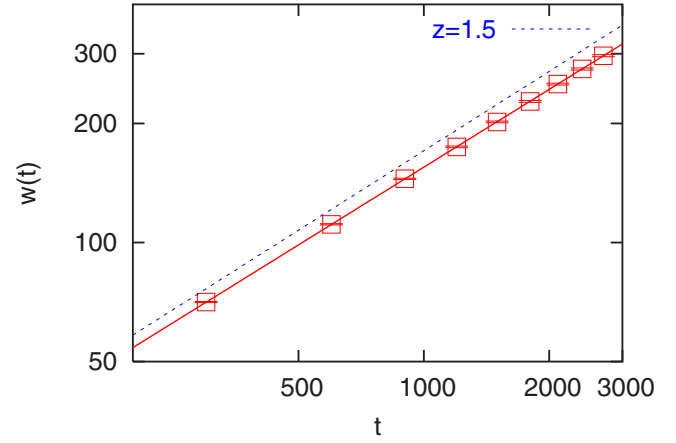


FIG. 7. (Color online) Widths and heights of the wave packets in $\mathcal{G}_{+-}(x,t)$ at series of time t for $p=r=1.0$ and $L=3200$. A line corresponding to $z=1.5$ is drawn above the data points in the upper figure.

$$W(x)^2 = x(\rho_+ - \rho_+^2) + x(\rho_- - \rho_-^2) = W(x; +)^2 + W(x; -)^2. \quad (7)$$

The square of the full interface width is thus equal to the sum of the squared interface widths in the two projected subspaces at $x \gg \xi$. The two coupled Burgers equations behave independently at length scales $x \gg \xi$.

C. Dynamic exponent from $\mathcal{G}_{+-}(x,t)$

Figure 6 shows the time evolution of the \mathcal{G}_{+-} correlation function starting from an initial uncorrelated disordered state (a δ function with a finite-size offset). The buildup of the cluster of $-$ particles in front of the tagged $+$ particle requires only a short time span τ_0 . The buildup of this surplus is mirrored by the buildup of a depletion layer behind the $+$ particle (particle numbers are locally conserved). After the screening cloud at $x > 0$ is fully established, $t > \tau_0$, the depletion packet detaches from $x=0$ and travels to the left. This traveling wave packet belongs to one of the two projected single-species ASEP subspaces and therefore should spread in time with KPZ dynamic exponent $z=3/2$ as $w \sim t^{1/z}$. The Gaussian form

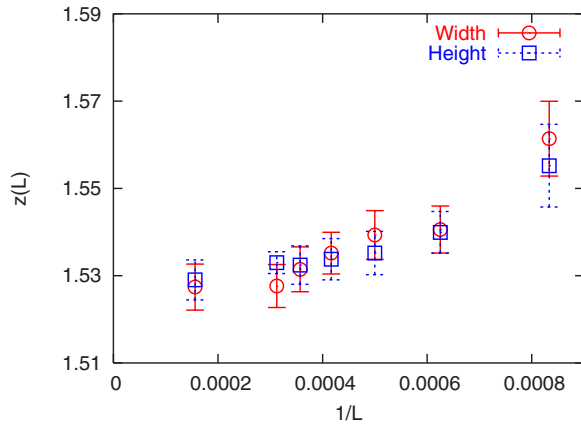


FIG. 8. (Color online) The estimates of the dynamic exponent z for finite system sizes $L=1200, 1600, 2000, 2400, 2800, 3200, 6400$. Analyses of finite-size correction to the scaling shows the estimate of dynamic exponent is equal to $1.53[2]$.

$$\delta\mathcal{G}_{+-}(x,t) \sim t^{-1/z} \exp\left[-\frac{(x-v_g t)^2}{Dt^{2/z}}\right],$$

fits the wave packet very well [21] except at times close to $t=\tau_0=\xi/v_g$, where it is slightly skewed. The packet's group velocity v_g follows the expected value $v_g=2p(1-2\rho)$, i.e., twice the group velocity of fluctuations in the $-$ or $+$ sector single-species ASEP. ($2v_g$ is the relative velocity of fluctuations in the $+$ and $-$ sectors, respectively, propagating in opposite directions.) The traveling depletion wave packet moves around the ring while broadening. It collides after one period with the screening cloud. They split off again. This keeps repeating itself, until the broadening has spread all over the ring and cancels out against the global finite scaling offset of the initial state.

Figure 7 shows the time evolution of the width of the wave packet w and its height h . They obey power laws: $w \sim t^{1/z}$ and $h \sim t^{-1/z}$. From these, we obtain estimates for the dynamic exponent z , and Fig. 8 shows the finite-size scaling behavior of these estimates. They converge to $z=1.53[2]$, consistent with the expected KPZ value $z=3/2$. This confirms that this way for determining z works well.

V. DYNAMIC SCREENING AT $r \neq p$

The correlation functions \mathcal{G}_{+-} and \mathcal{G}_{++} take more intricate shapes away from the $r=p$ line. Remarkably, as we will discuss next, this variety of shapes convert back into the simple shapes of $r=p$ using a quasiparticle representation. We discovered this numerically, as presented in this section, and then proved it analytically, as presented in the next section. The properties at the $r=p$ line, perfect screening between particles of opposite charge, and uncorrelated disordered stationary state statistics in the two projected subspaces, extend thus to all r/p in terms of quasiparticles, and the final conclusion from this is that the process factorizes into (KPZ)² everywhere for all r/p .

A. Stationary-state correlation functions

Figure 9 shows the \mathcal{G}_{+-} and \mathcal{G}_{++} correlators for various values of r/p . Compared to the $r=p$ shapes, \mathcal{G}_{+-} develops correlations at $x < 0$, and $\mathcal{G}_{++}=\mathcal{G}_{--}$ changes from a δ function into a symmetric correlated shape. This can be explained qualitatively as follows. At $r \neq p$, the $+$ and $-$ particles cannot choose to be blind with respect to each other anymore. Additional correlations buildup compared to the $r=p$ baseline behavior.

At $r < p$ the passing versus hopping rate is reduced. The screening cloud at $x > 0$ in \mathcal{G}_{+-} therefore grows (the clustering is stronger). This enhanced \mathcal{G}_{+-} screening cloud at $x > 0$, results in short-range correlations between alike particles as well; $\mathcal{G}_{++}(x)=\mathcal{G}_{--}(x)$ develops positive tails. This is a second-order effect. Those $++$ particle correlations in turn induce positive correlations in $\mathcal{G}_{+-}(x)$ for $x < 0$. This is a third-order effect, and thus an order of magnitude further down.

At $r > p$ the passing rate is enhanced with respect to the $r=p$ baseline behavior. The $x > 0$ screening cloud in $\mathcal{G}_{+-}(x)$ is thus smaller than at $r=p$. The correlations in $\mathcal{G}_{++}=\mathcal{G}_{--}$ are indeed negative, and represent a reduced probability to find alike particles near each other. This reduced probability makes it less likely to find $+$ particles behind the tagged $+$ particle, at $x < 0$. If those $+$ particles had been there, they would carry smaller screening clouds in front of them. Their absence therefore creates still positive correlations between $-$ particles at $x < 0$ and the tagged $+$ one.

At $r=2p$ the stationary state is fully disordered [14], the clustering vanishes, and all correlation functions reduce there to δ functions. At $r > 2p$ the correlation tails reemerge, but with opposite signs.

B. Dynamic exponents from $\mathcal{G}_{+-}(x,t)$ and $\mathcal{G}_{++}(x,t)$

We examine the temporal evolution of $\mathcal{G}_{+-}(x,t)$ and $\mathcal{G}_{++}(x,t)$ using MC simulations, just as we did in the $r=p$ case. The initial states are prepared to be uncorrelated and disordered. As shown in Fig. 10, two wave packets appear, with different amplitudes, but moving in opposite directions with the same speed. The wave packets in \mathcal{G}_{+-} are strongly coupled to those in \mathcal{G}_{++} . These traveling clouds are generated by the same type of mechanism as the one at $r=p$, i.e., the result of the rather fast buildup of the screening clouds near the tagged particle, reflected by the short-distance correlations in the stationary state. Both traveling clouds are mixtures of $+$ and $-$ particles, with nonzero projections in both \mathcal{G}_{++} and \mathcal{G}_{--} .

Once the clouds are detached from $x=0$, they move independently of each other in opposite directions, just as at $r=p$. The process factorizes again. But there is no *a priori* reason why these mixed traveling clouds at $r \neq p$ should spread as in pure KPZ. However, they do. In our MC simulations they spread, e.g., at $r=0.5$, $p=1.0$, and $\rho=0.25$, with $z=1.54[2]$ and at $r=0.7$, $p=1.0$, and $\rho=0.25$ with $z=1.51[2]$. Figures 11 and 12 show strong finite-size corrections to the scaling in the dynamic exponents, but the limiting behavior is clear.

Moreover, at $r=2p$, the stationary state is totally uncorrelated and disordered (and the temporal evolutions of the cor-

relation functions therefore do not involve traveling wave packets). We can apply the conventional method to estimate the dynamic exponent. The temporal evolution of the interface widths (see Figs. 13 and 14), yields $z=1.51[1]$.

C. Perfect screening in the quasiparticle representation

If indeed the dynamic exponent retains (KPZ)²-type value at $r \neq p$ as suggested by the above numerical results, then there might be a quasiparticle description in which the process factorizes at large length scales and in which the fluctuations are perfectly screened, just as at $r=p$. We found such a description, first numerically as described here, and then rigorously analytically in the following section. This implies the process obeys (KPZ)² scaling everywhere. In terms of quasiparticles the dynamic process fully factorizes into two KPZ processes at large coarse-grained scales.

Consider the stationary-state correlation functions in Figs. 9 and 10: the correlation functions decay to $1/L$ -type finite-size scaling offsets. The area A underneath \mathcal{G}_{++} for $x > 0$, the area B underneath \mathcal{G}_{++} at $x > 0$ (equal to the same for $x < 0$) and the area C underneath \mathcal{G}_{+-} for $x < 0$ obey empirically the relation $B/A=C/B$, for all $r \neq p$, typically with a numerical accuracy $1-B^2/AC=0.01\%$. (The areas are measured with respect to the offsets.)

This special balance in the areas relates to a specific amount of mixing between $+$ and $-$ particles in the clouds, and suggests (a much stronger property) the existence of a quasiparticle representation,

$$n_p = \alpha n_+ + \beta n_-, \quad n_m = \beta n_+ + \alpha n_-, \quad (8)$$

with n_{\pm} the number operator for $+$ and $-$ particles and

$$\frac{\beta}{\alpha} = \frac{B}{A} = \frac{C}{B}, \quad (9)$$

in which the correlation functions $\mathcal{G}_{pp}(x)=\mathcal{G}_{mm}(x)$ and $\mathcal{G}_{pm}(x)$, defined as

$$\mathcal{G}_{\nu\mu}(x) \equiv \langle n_{\nu}(0)n_{\mu}(x) \rangle - \langle n_{\nu}(0) \rangle \langle n_{\mu}(x) \rangle, \quad (10)$$

with $\nu, \mu = p, m$ reduce to the same shapes as the particle correlators at $r/p=1$ [where $\mathcal{G}_{pp}(x)$ is a δ function and \mathcal{G}_{pm} has only one tail and shows perfect screening between quasiparticles of opposite charges].

The mixing ratio $R=\beta/\alpha$ varies from $R=\beta/\alpha=0$ at $r=p$ (with $n_p=n_+$ and $n_m=n_-$); to $R=\beta/\alpha=1$ when $n_p=n_m$, and to $R=\beta/\alpha=-1$ when $n_p=-n_m$. Figure 15 shows lines of R from our analytic expression in Sec. VI F. Our numerical results are completely consistent with this. The mixing strength increases with density ρ , and becomes indeterminate at the line

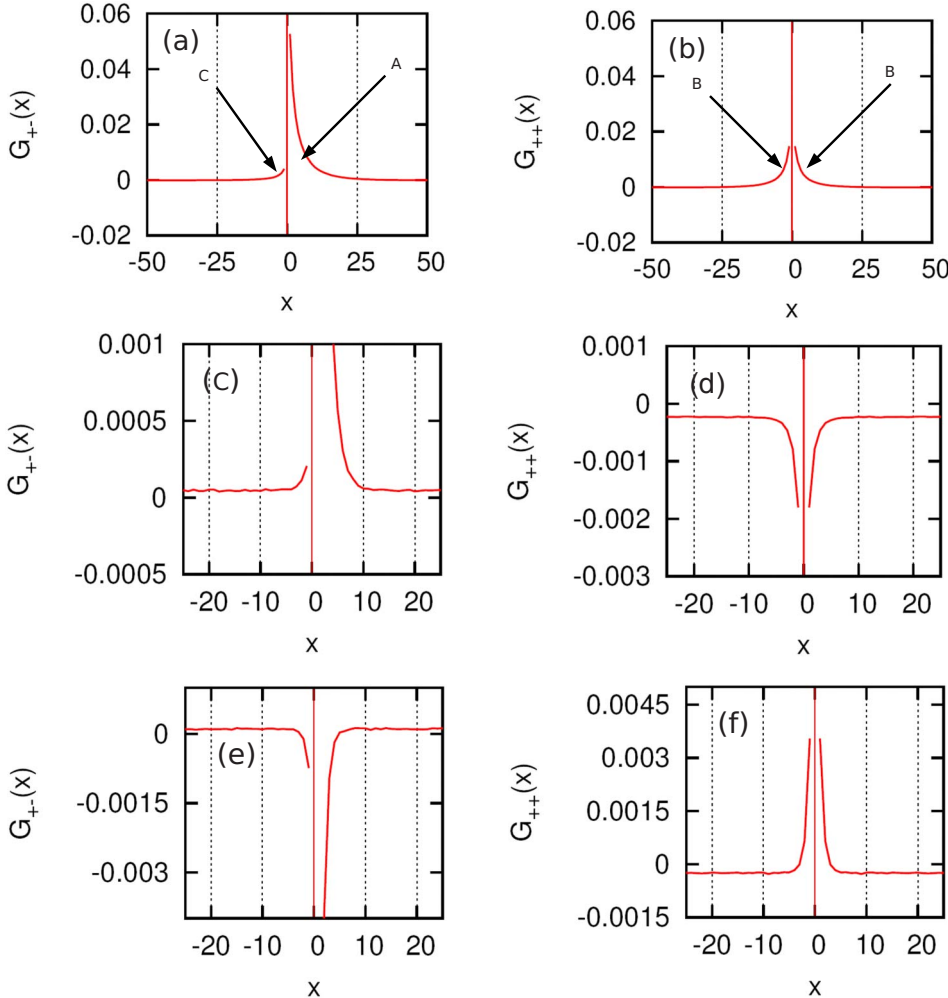


FIG. 9. (Color online) Stationary correlation functions $\mathcal{G}_{+-}(x)$ (left column) and $\mathcal{G}_{++}(x)$ (right column), for $p=1.0$, $r=0.5$, and $\rho=0.25$ for $L=3200$ [(a) and (b)], $p=0.7$, $r=1.0$, and $\rho=0.25$ for $L=800$ [(c) and (d)], and $p=0.3$, $r=0.9$, and $\rho=0.25$ for $L=800$ [(e) and (f)].

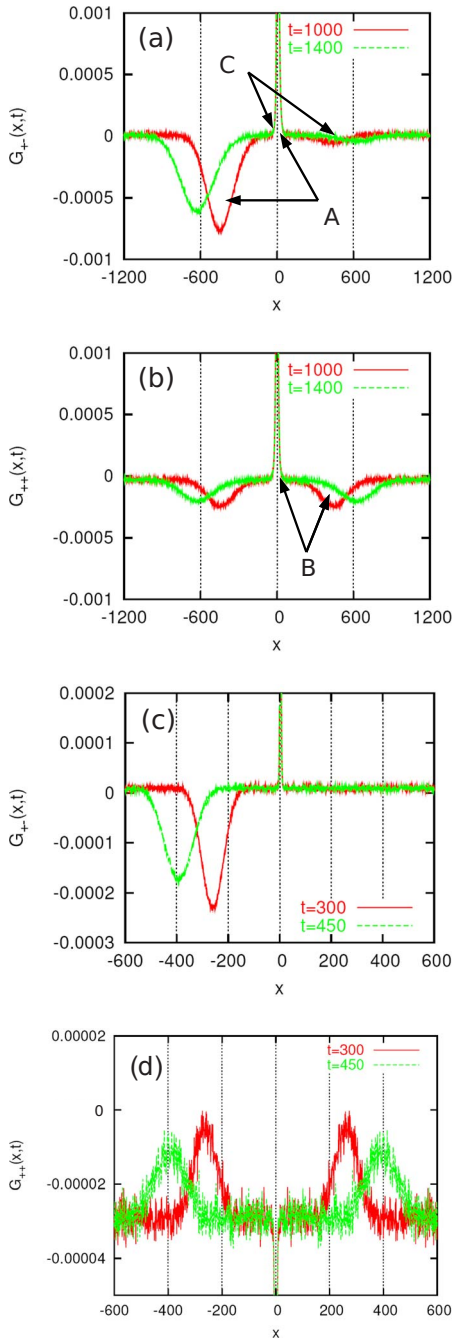


FIG. 10. (Color online) (a) Correlation function between + and - at $t=1000$ and 1400 with $p=1.0$, $r=0.5$, and $L=6400$. The initial state is random disordered. (b) The corresponding correlation function between + and +. (c) $G_{+-}(x,t)$ for $t=300, 450$ with $p=0.7$, $r=1.0$, and $L=6400$. (d) The corresponding $G_{++}(x,t)$.

$\rho=0.5$, where all sites are fully occupied. At $r/p=2$ the stationary state is totally disordered, but R does not vanish since + and - remain strongly correlated dynamically [22]. Both α and β go to zero and change sign across the $r/p=2$ line.

VI. PERFECT SCREENING AND THE MATRIX PRODUCT STATIONARY-STATE STRUCTURE

In this section, we prove analytically the perfect screening of the (quasiparticles) pair correlators, using the matrix prod-

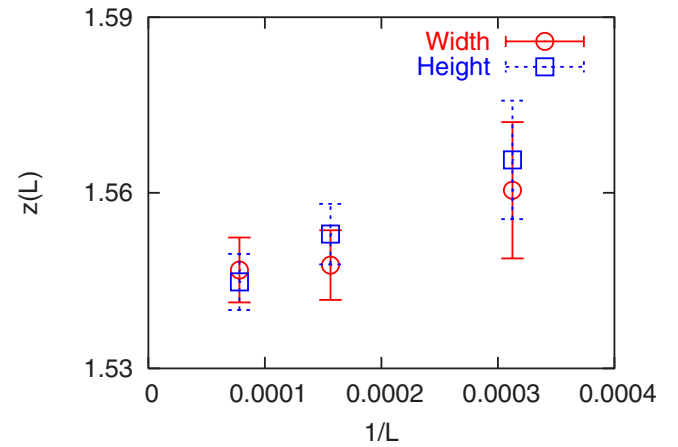


FIG. 11. (Color online) The estimates of dynamic exponent z for different system sizes at $p=1.0$, $r=0.5$, and $\rho=0.25$.

uct ansatz (MPA) structure of the stationary state. The proof applies to all r/p , but for clarity we split up the discussion. First, we review briefly the general properties of MPA stationary states. Next, we present the proof at $r=p$, and finally generalize it to all r/p in terms of quasiparticles.

A. MPA-type stationary states

Stationary states of stochastic dynamic processes are typically very complex with intricate long-range effective interactions between the degrees of freedom (when writing the stationary state in terms of effective Gibbs-Boltzmann factors). The long-range aspect is important; 1D driven stochastic processes can undergo nontrivial phase transitions, while 1D equilibrium degrees of freedom with short-range interactions cannot. MPA states are linked to equilibrium distributions and therefore lack long-range correlations.

MPA stationary states are of the form [14,15,17]

$$P_s(\{\tau_{ij}\}) = \frac{1}{Z} \text{Tr}[G_{\tau_1} G_{\tau_2} \cdots], \quad (11)$$

with in our case $\tau_i = +, 0, -$. This structure resembles closely the transfer-matrix formulation of partition functions in one

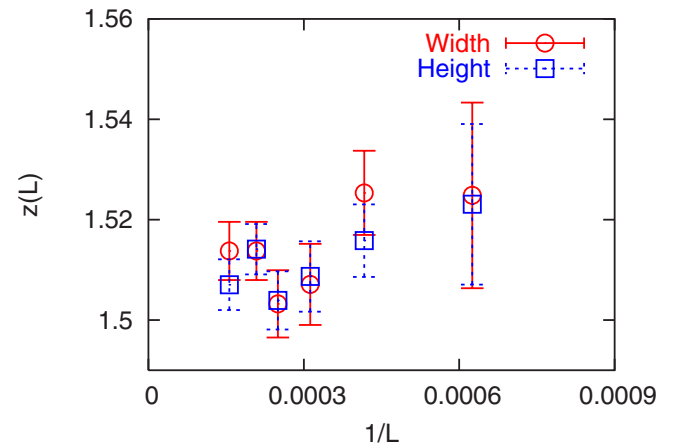


FIG. 12. (Color online) The estimates of dynamic exponent z for different system sizes at $p=0.7$, $r=1.0$, and $\rho=0.25$.

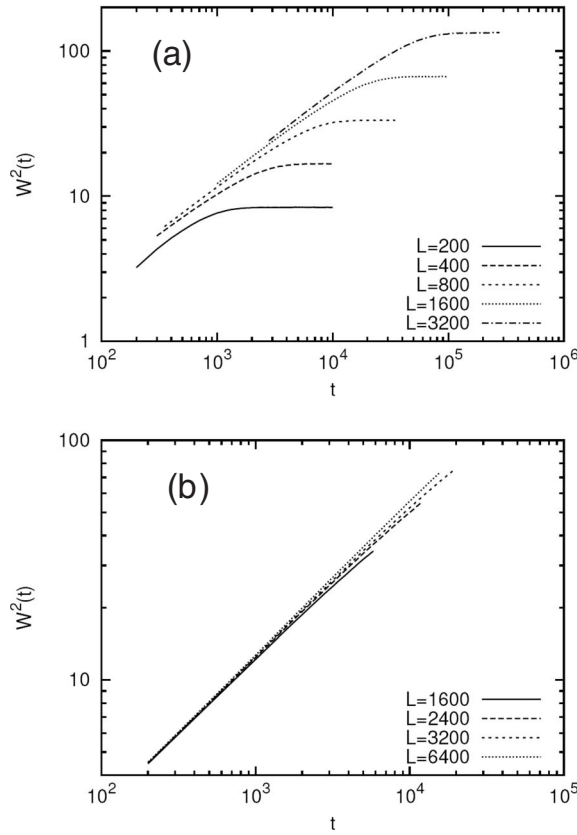


FIG. 13. The temporal evolution of the interface widths starting from initial flat interfaces for $p=0.5$, $r=1.0$, and $\rho=0.25$. (a) The evolution of the widths for different system sizes only shows oscillations for $t < 200$. (b) The dynamic exponent is estimated by measuring the slopes of log-log plot of the interface width vs time.

dimensional (1D) equilibrium statistical mechanics. Consider, for example, a one-dimensional Ising model, with spin $S = \pm 1$ degrees of freedom at sites $i + \frac{1}{2}$, that interact as

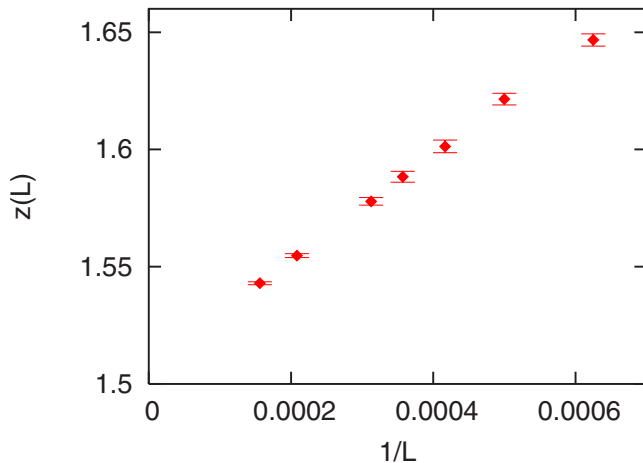


FIG. 14. (Color online) The estimate of dynamic exponent z for different system sizes at $p=0.5$, $r=1.0$, and $\rho=0.25$.

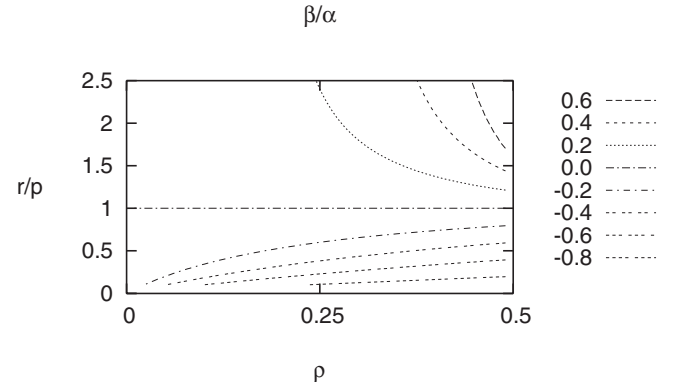


FIG. 15. Contour plot of β/α in a parameter space of r/p and ρ [see Eq. (49)].

$$E = \sum_i K(\tau_i) S_{i+1/2} S_{i-1/2}, \quad (12)$$

and with a degree of freedom $\tau_i = 0, \pm 1$ on every bond i such that bond energy $K(\tau_i)$ can have three distinct values. In that case, the G_{τ_i} are 2×2 transfer matrices and the stationary-state probability for the yet unrelated stochastic dynamic process is the Ising equilibrium partition function for a given $\{\tau_i\}$ configuration,

$$P_s(\{\tau_i\}) = \sum_{\{S\}} e^{-E(\{\tau, S\})}. \quad (13)$$

The normalization factor

$$\mathcal{Z} = \sum_{\{\tau_i\},*} P_s(\{\tau_i\}) \quad (14)$$

is the canonical partition function of the annealed random bond 1D Ising model. The stochastic driven nonequilibrium dynamics typically imposes constraints on the τ_i degrees of freedom. In our dynamic process the number of each species of particle $\tau = \pm$ is conserved independently. This is denoted by * in Eq. (14).

The τ variables do not couple to each other directly in Eq. (13); all correlations between τ degrees of freedom are mediated by the Ising field S_x . The search for a possible MPA structure of the stationary state is therefore the search for the existence of a representation in which all correlations between the original τ degrees of freedom are carried by a new auxiliary field and expressed as short-range interactions between those new degrees of freedom. Those auxiliary degrees of freedom can take any form, not just Ising spins, because the rank of the G matrices and their symmetries can be arbitrary. For example, in our case, the rank will be infinite, and the auxiliary field can be interpreted as (integer-valued) interface-type degrees of freedom, denoted as $n_x = 0, \pm 1, \pm 2, \dots$

The transfer-matrix product structure, Eq. (11), implies that those auxiliary degrees of freedom interact by nearest-neighbor interactions only. This is actually unfortunate, because in short-ranged 1D equilibrium systems, such as Eq. (13), spontaneous broken symmetries and phase transitions are impossible. Therefore, master equations with MPA sta-

tionary states have at best dynamic phase transitions with trivial scaling properties (associated with an abrupt change in the G representation). For example, MPA representations of directed percolation or directed Ising-type processes cannot exist, because both are believed to have transitions with complex scaling dimensions. Still, the MPA method has been proved to be a powerful tool, its algebraic structure is very elegant, and a surprisingly large class of 1D stochastic dynamic processes have a MPA-type stationary state.

Boundary conditions play an important role. Equation (14) is a canonical partition function, where the number of + and - particles are each conserved. Consider instead the generating function

$$\mathcal{Z} = \sum_{\{\tau_i\}} z_-^{N_-} z_+^{N_+} P_s(\{\tau_i\}) = \text{Tr}[(z_+ G_+ + z_- G_- + G_0)^L] = \text{Tr}[M^L], \quad (15)$$

with

$$M = z_+ G_+ + z_- G_- + G_0. \quad (16)$$

This would be the grand canonical partition function of, e.g., the above annealed random bond 1D Ising model in case of periodic boundary conditions. z_{\pm} are the fugacities of the τ_{\pm} particles. The equivalence between the ensembles in the thermodynamic limit is ensured in the equilibrium interpretation, where the details of how the particle reservoirs couple to the system does not have to be addressed. This is different in the interpretation of the MPA as the stationary state of a driven stochastic process. Dynamic processes are very sensitive to boundary conditions. For example, a process with open boundary conditions and reservoirs at the edges conserves the number of particles everywhere inside the bulk, and behaves very differently from the one where the reservoirs couple directly to every site. Not surprisingly, therefore, the MPA method only applies to the stationary state; the introduction of the auxiliary field does not address the stochastic dynamics, nor the temporal fluctuations in the stationary state. For periodic boundary conditions, as in our case, the grand canonical partition function, Eq. (15), represents an ensemble of dynamic systems, each with periodic boundary condition systems, and fixed values of N_- and N_+ , weighted with respect to each other by the fugacity probability factor. In this sense the ensembles are equivalent in the thermodynamic limit. In our discussion below we use the grand canonical ensemble. The correlation functions for $x > 0$ are evaluated then as

$$G_{+-}(x) = \frac{1}{\lambda_B^2} \left[\langle B | G_+ \left(\frac{M}{\lambda_B} \right)^{x-1} G_- | B \rangle - \langle B | G_+ | B \rangle \langle B | G_- | B \rangle \right] \quad (17)$$

in the thermodynamic limit, with $|B\rangle$ and $\langle B|$ the right and left eigenvectors of the largest eigenvalue λ_B of the operator M defined in Eq. (16). The correlator at $x=0$, $\langle n_+ n_- \rangle$, poses somewhat of a problem. It cannot be expressed as simple as this due to the intrinsic off-diagonal character of the above G operators. At $r=p$ this is not an issue, because $\langle n_+ n_- \rangle = 0$.

However, that will not be true anymore for the quasiparticles at $r \neq p$.

B. Quadratic algebra

The first step in identifying whether the stationary state of a stochastic process might have a MPA structure, is to insert Eq. (11) into the master equation. If lucky, the condition of stationarity can be expressed as simple algebraic conditions on the G_{τ} transfer matrices. The MPA structure of our process has been studied extensively recently [14–19]. From those studies we know that the three G_{τ} must obey the quadratic algebra as follows:

$$\begin{aligned} r G_+ G_- &= -x_- G_+ + x_+ G_-, \\ p G_+ G_0 &= -x_0 G_+ + x_+ G_0, \\ p G_0 G_- &= -x_- G_0 + x_0 G_-, \end{aligned} \quad (18)$$

with x_0 and x_{\pm} arbitrary yet unspecified parameters. These conditions apply to the entire phase diagram, for all r/p . The next step is to find explicit representations of the G_{τ} that satisfy Eq. (18), using the freedom in choice of the parameters x_i . In general, the rank of the G_{τ} does not close, but remains infinite. The rank is finite only along special lines in the phase diagram. Fortunately, for our purposes we do not need closure; the quadratic algebra structure itself is sufficient to prove perfect screening.

Our process is invariant under simultaneous inversion in space $x \rightarrow -x$ and of charge $+ \leftrightarrow -$ in the case that the numbers of + and - particles are balanced. This suggests we look for a realization of the algebra with operators satisfying $G_+ = G_-^T$ and $G_0 = G_0^T$. This invariance is valid in the subspace $x_+ = -x_- = r$ and $x_0 = 0$ [14], where the quadratic algebra reduces to

$$\begin{aligned} G_+ G_- &= G_+ + G_-, \\ G_+ G_0 &= G_0 G_- = \frac{r}{p} G_0. \end{aligned} \quad (19)$$

C. $r=p$ quadratic algebra

At $r=p$, the quadratic algebra of Eq. (19) is easily checked to be satisfied by the operators [15]

$$G_+ = I + L_-, \quad G_- = I + L_+, \quad G_0 = |0\rangle\langle 0|. \quad (20)$$

The rank of these matrices is infinite. The auxiliary degrees of freedom are (positive only) integer-valued “height variables” $n=0, 1, 2, \dots$. G_0 is the projection operator onto the $n=0$ state, and L_{\pm} are the raising (lowering) operators $L_{\pm}|n\rangle = |n \pm 1\rangle$.

We need to determine the eigenvalues of the grand canonical transfer matrix, Eq. (16),

$$M = z G_+ + z G_- + G_0 = z(2I + L_+ + L_-) + G_0. \quad (21)$$

This matrix has several interpretations. It is the transfer matrix for the equilibrium partition function of a one-

dimensional interface in the presence of a substrate (all $n < 0$ are excluded) with a short-range attractive potential at $n=0$; like a substrate. Such an interface layer is thin and nonrough. It is also the time evolution of a 1D random walker (with x playing the role of time and n that of space) in half space, $n \geq 0$ and an on-site attractive interaction at site $n=0$. Such a random walker is localized. The latter can be presented also as the localization of a single quantum mechanical particle hopping on a semi-infinite chain with a δ -function attractive potential at the first site,

$$H \equiv 2I - L_+ - L_- - \frac{1}{z}G_0, \quad (22)$$

with $M=4z(1-\frac{1}{4}H)$.

This simple Hamiltonian has one single bound state and a continuum spectrum of extended states. The calculation of the eigenspectrum is elementary and straightforward. The eigenstates $|\lambda\rangle=(\phi_0, \phi_1, \dots)$, satisfy the equations

$$\begin{aligned} \left(2 - \frac{1}{z}\right)\phi_0 - \phi_1 &= E\phi_0, \\ -\phi_{n-1} + 2\phi_n - \phi_{n+1} &= E\phi_n \quad \text{for } n \geq 1. \end{aligned} \quad (23)$$

Bound states have the generic form

$$\phi_n = \frac{1}{\sqrt{Z_B}} w_b^n \quad \text{for } n \geq 0. \quad (24)$$

Substitution in Eq. (23) yields only one bound state, with energy $E_B=2-1/w_b-w_b$, such that

$$\lambda_B = \frac{z}{w_b}(1+w_b)^2, \quad (25)$$

and normalization

$$Z_B = \frac{1}{1-w_b^2}. \quad (26)$$

w_b is equal to $w_b=z$.

The extended eigenstates are scattered waves, with

$$\phi_0 = \frac{A_0(k)}{\sqrt{Z(k)}}, \quad \phi_n = \frac{1}{\sqrt{Z(k)}} \cos(kn + \theta_k). \quad (27)$$

The eigenvalue equations at $n > 1$ yield the energy spectrum $E(k)=2(1-\cos k)$, with $0 < k < \pi$, such that

$$\lambda(k) = 2z(1 + \cos k), \quad (28)$$

and those at $n=0, 1$ yield the phase shift θ_k ,

$$A_0(k) = \cos(\theta_k) = z \cos(\theta_k - k) = \frac{z \cos(\theta_k + k)}{2z - zE_k - 1}. \quad (29)$$

The normalization factor

$$|\phi_0|^2 + \sum_{n=1}^D |\phi_n|^2 = 1 \rightarrow Z(k) = |A_0|^2 + \frac{1}{2}D \quad (30)$$

is proportional to the rank of the matrices D , and thus strictly speaking infinite; D will drop out in our calculations below.

The $n=0$ component is easily evaluated as follows:

$$\phi_0^2 = |\langle 0|k\rangle|^2 = \frac{2}{D} \frac{z^2 \sin^2 k}{z^2 - 2z \cos k + 1}. \quad (31)$$

D. Perfect screening at $r=p$

Perfect screening implies that

$$\sum_{x=1}^{\infty} \mathcal{G}_{+-}(x) = -\mathcal{G}_{+-}(0), \quad (32)$$

i.e., that the sum over $x > 0$ of the correlator Eq. (17),

$$S = \sum_{x=1}^{\infty} \mathcal{G}_{+-}(x) \quad (33)$$

is equal to the right-hand side of Eq. (32),

$$S = \rho^2 = z^2 \left(\frac{\lambda_p}{\lambda_B} \right)^2, \quad (34)$$

with $\rho = z\lambda_p/\lambda_B$, using that the bound state is also an eigenstate of G_+ , $G_+|B\rangle = \lambda_p|B\rangle = (1+w_b)|B\rangle$. In our specific case the density is simply equal to $\rho = z/(1+z)$, but we like to keep the derivation as generic as possible.

We need to demonstrate that this sum rule is valid in the thermodynamic limit, and track carefully any terms that scale as system size L . For example, as discussed already in detail above, the sum rule is trivially true for periodic boundary conditions, but then does not imply perfect screening, because any unscreened surplus can be spread out over the entire lattice in the form of a $1/L$ background density.

Define $P_B = |B\rangle\langle B|$, as the projection operator onto the bound state, and rewrite Eq. (17), as

$$S = \sum_{x=1}^D \mathcal{G}_{+-}(x) = \frac{z^2}{\lambda_B^2} \langle B|G_+ \sum_{x=1}^D \left[\left(\frac{M}{\lambda_B} \right)^{x-1} - P_B \right] G_-|B\rangle. \quad (35)$$

The bound state does not contribute to the correlators inside the sum. Therefore we can project out the bound state from M and then perform the summation

$$\begin{aligned} S &= \frac{z^2}{\lambda_B^2} \langle B|G_+ \left[\sum_{x=1}^D \left(\frac{M}{\lambda_B} - P_B \right)^{x-1} - P_B \right] G_-|B\rangle \\ &= \frac{z^2}{\lambda_B^2} \langle B|G_+ \left[\frac{1}{1 - \frac{M}{\lambda_B} + P_B} - P_B \right] G_-|B\rangle. \end{aligned} \quad (36)$$

(The single P_B outside the summation originates from the $x=1$ contribution.) We can remove G_+ and G_- from the above equation, because the bound state is also an eigenstate of the lowering operator $G_+|B\rangle = \lambda_p|B\rangle$,

$$S = \frac{|\langle B|0\rangle|^2}{\lambda_B^2} \langle 0| \left[\frac{1}{1 - \frac{M}{\lambda_B} + P_B} - P_B \right] |0\rangle, \quad (37)$$

writing $zG_{\pm} = M - G_0 - zG_{\mp}$, and using that $G_0 = |0\rangle\langle 0|$ is the projection operator onto the first site, and also that $M - \lambda_B P_B$ has no projection onto $|B\rangle$.

The sum rule we seek is now reduced to the identity

$$\sum_{k \neq B} \frac{|\langle 0|k\rangle|^2}{\lambda_B - \lambda_k} = \frac{z^2 \lambda_p^2}{\lambda_B \lambda_0}, \quad (38)$$

with $\lambda_0 = |\langle B|0\rangle|^2 = \langle B|G_0|B\rangle = \langle B|M - z(G_+ + G_-)|B\rangle = \lambda_B - 2z\lambda_p$. The left-hand side is easily evaluated, using Eq. (31) and that $\lambda_B - \lambda_k = z^2 - 2z \cos k + 1$,

$$\sum_{k \neq B} \frac{|\langle 0|k\rangle|^2}{\lambda_B - \lambda_k} = \frac{2}{\pi} \int_0^{\pi} dk \frac{z^2 \sin^2 k}{(z^2 - 2z \cos k + 1)^2}. \quad (39)$$

This is an elementary contour integral along the unit circle in the complex $w = e^{ik}$ plane, with a double pole at $w = w_b = z$ within the circle in addition to a single pole at $w = 0$. The integral is indeed equal to $z^2/(1 - z^2)$, the right-hand side of Eq. (37) [$\lambda_p^2 = \lambda_B = (1 + z)^2$ and $\lambda_0 = 1 - z^2$].

E. Quadratic algebra at $r \neq p$

The proof of perfect screening for general r/p follows the same pattern as at $r=p$. The operators obeying the quadratic algebra conditions, Eq. (19), are again expressed in terms of raising and lowering operators L_{\pm} [14–19],

$$\begin{aligned} G_+ &= \frac{1}{a} [I + L_- + (a-1)G_0 + (s-1)G_0 L_-], \\ G_- &= \frac{1}{a} [I + L_+ + (a-1)G_0 + (s-1)L_+ G_0], \\ G_0 &= |0\rangle\langle 0|, \end{aligned} \quad (40)$$

where $a = r/p$ and $s^2 = 1 - (a-1)^2$. The transfer matrix retains its form,

$$M = zG_+ + zG_- + G_0 = \frac{4z}{a} \left(1 - \frac{1}{4}H \right), \quad (41)$$

with modified Hamiltonian,

$$H \equiv 2I - L_+ - L_- - \frac{1}{z}G_0 - (s-1)(G_0 L_- + L_+ G_0), \quad (42)$$

and with $1/\bar{z} \equiv a/z + 2(a-1)$. This is again a one-dimensional single-particle hopping process in a half space, $n = 0, 1, 2, \dots$. Compared to Eq. (22) for $a = \frac{r}{p} = 1$, the attractive potential at site $n=1$ deepens for $r > p$ (reducing the clustering and correlation lengths). The novel element is the modified hopping probability s between sites $n=1$ and $n=0$. There is still only one bound state

$$\phi_n = \frac{1}{\sqrt{Z_B}} w_b^n \quad \text{for } n \geq 1,$$

$$\phi_0 = \frac{1}{\sqrt{Z_B}} \frac{1}{s},$$

$$\frac{1}{\bar{z}} = \frac{1}{w_b} + (1 - s^2)w_b, \quad (43)$$

with the same functional form for the bound-state energy as before, Eq. (25).

The derivation of the extended states is also straightforward. They are again of the form, Eq. (27), with the same energies, $E_k = 2(1 - \cos k)$, but satisfying the modified relations

$$sA_0(k) = \cos(\theta_k) = \frac{s^2 \cos(\theta_k + k)}{2 \cos k - \frac{1}{\bar{z}}}. \quad (44)$$

This leads after some algebra to

$$\phi_0^2 = \frac{(w_b' w_b - 1) \sin^2 k 2/D}{(w_b + w_b^{-1} - 2 \cos k)(w_b' + w_b'^{-1} - 2 \cos k)}. \quad (45)$$

w_b' is the second root of the bound-state equation, Eq. (43).

F. Quasiparticle representation

We can now identify the exact form of the ratio α/β in the quasiparticle representation, Eq. (8). The representation mixes the G_{\pm} operators in Eq. (40) as

$$G_p = \alpha G_+ + \beta G_-, \quad G_m = \beta G_+ + \alpha G_-. \quad (46)$$

The projection operator $G_0 = |0\rangle\langle 0|$, and the transfer matrix M are invariant. The latter implies $\alpha + \beta = 1$.

The quasiparticle two-point correlation functions take the same form as the particle correlators at $r=p$. In particular, the quasiparticle correlation function $\mathcal{G}_{pm}(x)$ is zero for all $x < 0$. This is true when the bound state is also an eigenstate of G_p as follows:

$$G_p |B\rangle = \lambda_p |B\rangle. \quad (47)$$

Inserting the bound state, Eq. (43), yields

$$a\lambda_p = 1 + \alpha w_b + \frac{\beta}{w_b}, \quad (48)$$

and

$$\frac{\beta}{\alpha} = \frac{(s^2 - 1)w_b - (1 - a)}{1/w_b + (1 - a)}. \quad (49)$$

The lines of constant β/α are shown in Fig. 15. (Insert the above equations for w_b , \bar{z} , and the relation between a and s .) The contours coincide with our numerical results.

G. Perfect screening at $r \neq p$

The final step is to prove perfect screening in terms of the quasiparticles as follows:

$$S = \sum_{x=1}^{\infty} \mathcal{G}_{pm}(x) = -\mathcal{G}_{pm}(0). \quad (50)$$

The left-hand side reduces to exactly the same form as Eq. (37), using the exact same steps, because the bound state is an eigenstate of G_p just like the particle operator G_+ at $r=p$; that is all we used there. The right-hand side is different, because $\langle n_p n_m \rangle = 2\alpha\beta\rho$ is not zero anymore. Since $\alpha+\beta=1$, it is still true that $\rho_p = \rho_m = \rho_+ = \rho_- = z\lambda_p/\lambda_B$. Therefore, the sum rule equation, Eq. (38), now takes the form

$$\sum_{k \neq B} \frac{|\langle 0|k \rangle|^2}{\lambda_B - \lambda_k} = \frac{1}{\lambda_0} \left(\frac{z^2 \lambda_p^2}{\lambda_B} - 2\alpha\beta z \lambda_p \right), \quad (51)$$

with, as before, $\lambda_0 = |\langle B|0 \rangle|^2 = \langle B|G_0|B \rangle = \langle B|M - z(G_p + G_m)|B \rangle = \lambda_B - 2z\lambda_p$. The summation on the left leads again to a $w=e^{ik}$ -type contour integral. It still has only two poles inside the unit circle: one double pole at $w=w_b$ and one single pole at $w=1/w'_b$ [with w'_b the second root of Eq. (43).] The result is indeed equal to the right-hand side after inserting the proper expressions for the various eigenvalues and some not very pretty algebra.

VII. RESULTS AND CONCLUSIONS

We have studied the two-species asymmetric exclusion process (ASEP) to determine whether the addition of a local conservation law changes the dynamic scaling properties. In the Burgers (hydrodynamics) context the process conserves both momentum and density. In the KPZ context it represents interface growth where the numbers of up and down steps are conserved. In the ASEP context the particle numbers of both species are conserved.

We find that the dynamic scaling exponent retains the KPZ $z=3/2$ value. The AHR process factorizes at scales larger than the clustering length scale ξ into two independent KPZ processes. At $r=p$, where the passing and hopping probabilities are equal, this factorization occurs in terms of + and - particles, while at $r \neq p$ it is established in terms of quasiparticles. This factorization expresses itself as perfect

screening between the two species of quasiparticles. ξ , the screening length, coincides with the clustering length scale and represents the crossover length scale between single KPZ scaling (within each cluster) and factorized (KPZ)²-type scaling.

The conventional method for measuring the dynamic exponents in simulations in terms of the time evolution of the interface width fails in this process due to the presence of time oscillations with a period proportional to the system size; quasiparticle fluctuations have nonzero and opposite drift velocities. Instead, we determined the dynamic scaling from the two-point correlation functions. This might be the first time that it is done in this manner.

The stationary state of this process has been studied extensively in the recent literature, because it obeys the so-called matrix product ansatz (MPA). We used this to prove rigorously the factorization of the fluctuations in terms of quasiparticles. This previously unknown feature of the algebraic structure of the MPA method needs to be understood better, in particular, in the context of clustering phenomena in general.

The perfect screening phenomenon is clearly a topological feature. The above presentation only partially exposes those topological properties; by bringing the perfect screening condition into the form of Eqs. (38) and (51). The right-hand sides of both equations only involve bound-state properties. Their left-hand sides, however, involve a summation over all extended states; i.e., their projections onto $n=0$ ($|\langle 0|k \rangle|^2$). The poles of the contour integral links this to the bound states and the quasiparticle mixing. The formulation of a general proof is important because, if topological, the perfect screening and (KPZ)² scaling at large length scales will be generic features, valid to many more processes with clustering. Its limitations can teach us when and how novel-type dynamic scaling sets in.

ACKNOWLEDGMENT

This research is supported by the National Science Foundation under Grant No. DMR-0341341.

-
- [1] H. Hinrichsen, *Adv. Phys.* **49**, 815 (2000).
 - [2] G. Ódor, *Rev. Mod. Phys.* **76**, 663 (2004).
 - [3] T. M. Liggett, *Interacting Particle Systems* (Springer-Verlag, New York, 1985).
 - [4] H. Spohn, *Large Scale Dynamics of Interacting Particles* (Springer-Verlag, New York, 1991).
 - [5] B. Schmittmann and R. K. P. Zia, *Statistical Mechanics of Driven Diffusive Systems, Phase Transitions and Critical Phenomena* (Academic, New York, 1995), Vol. 17.
 - [6] T. Halpin-Healy and Y.-C. Zhang, *Phys. Rep.* **254**, 215 (1995).
 - [7] S. Lepri, R. Livi, and A. Politi, *Phys. Rev. Lett.* **78**, 1896 (1997); *Europhys. Lett.* **43**, 271 (1998); *Phys. Rev. Lett.* **84**, 2857 (2000); *Phys. Rev. E* **68**, 067102 (2003); *Phys. Rep.* **377**, 1 (2003).
 - [8] P. Grassberger, W. Nadler, and L. Yang, *Phys. Rev. Lett.* **89**, 180601 (2002); G. Casati and T. Prosen, *Phys. Rev. E* **67**, 015203(R) (2003); J. M. Deutsch and O. Narayan, *ibid.* **68**, 010201(R) (2003).
 - [9] J. S. Wang and B. Li, *Phys. Rev. E* **70**, 021204 (2004); T. Hatano, *ibid.* **59**, R1 (1999).
 - [10] J. S. Wang and B. Li, *Phys. Rev. Lett.* **92**, 074302 (2004).
 - [11] O. Narayan and S. Ramaswamy, *Phys. Rev. Lett.* **89**, 200601 (2002); T. Mai and O. Narayan, *Phys. Rev. E* **73**, 061202 (2006).
 - [12] J. M. Burgers, *The Nonlinear Diffusion Equation* (Riedel, Boston, 1974).
 - [13] M. den Nijs (unpublished).
 - [14] P. F. Arndt, T. Heinzl, and V. Rittenberg, *J. Phys. A* **31**, 833

- (1998).
- [15] P. F. Arndt, T. Heinzl, and V. Rittenberg, *J. Stat. Phys.* **97**, 1 (1999).
- [16] Y. Kafri, E. Levine, D. Mukamel, G. M. Schütz, and J. Török, *Phys. Rev. Lett.* **89**, 035702 (2002).
- [17] N. Rajewsky, T. Sasamoto, and E. R. Speer, *Physica A* **279**, 123 (2000).
- [18] G. M. Schütz, *J. Phys. A* **36**, R339 (2003).
- [19] Y. Kafri, E. Levine, D. Mukamel, G. M. Schütz, and R. D. Willmann, *Phys. Rev. E* **68**, 035101(R) (2003).
- [20] M. R. Evans and T. Hanney, *J. Phys. A* **38**, R195 (2005).
- [21] The Levenberg-Marquardt method is used with a confidence bound of 95%.
- [22] V. Popkov and G. M. Schütz, *J. Stat. Mech.: Theory Exp.* **12**, P12004 (2004).